

Deep Doubly Debiased Longitudinal Effect Estimation with ICE G-Computation

Wenxin Chen

wc645@cornell.edu

Cornell University

New York, New York, USA

Kyra Gan

Cornell University

New York, New York, USA

Weishen Pan

Cornell University

New York, New York, USA

Fei Wang

Cornell University

New York, New York, USA

Abstract

Estimating longitudinal treatment effects is essential for sequential decision-making but is challenging due to treatment-confounder feedback. While *Iterative Conditional Expectation (ICE) G-computation* offers a principled approach, its recursive structure suffers from error propagation, corrupting the learned outcome regression models. We propose **D³-Net**, a framework that mitigates error propagation in ICE training and then applies a robust final correction. First, to interrupt error propagation *during learning*, we train the ICE sequence using *Sequential Doubly Robust (SDR) pseudo-outcomes*, which provide bias-corrected targets for each regression. Second, we employ a multi-task Transformer with a *covariate simulator head* for auxiliary supervision, regularizing representations against corruption by noisy pseudo-outcomes, and a *target network* to stabilize training dynamics. For the final estimate, we discard the SDR correction and instead use the uncorrected nuisance models to perform *Longitudinal Targeted Minimum Loss-Based Estimation (LTMLE)* on the original outcomes. This second-stage, targeted debiasing ensures robustness and optimal finite-sample properties. Comprehensive experiments demonstrate that our model, **D³-Net**, robustly reduces bias and variance across different horizons, counterfactuals, and time-varying confounders, compared to existing state-of-the-art ICE-based estimators.

CCS Concepts

- Computing methodologies → Neural networks; Causal reasoning and diagnostics; • Applied computing → Health informatics.

Keywords

longitudinal effect estimation, iterative conditional expectation, sequential doubly robust, targeted minimum loss-based estimation

1 Introduction

Clinical decision-making is often sequential, with treatments adapted over time based on a patient’s evolving status. Estimating the effect of a *sequence* of treatments is therefore crucial for informing optimal care. However, this longitudinal problem is fundamentally challenging due to the treatment-confounder feedback: time-varying confounders are affected by past treatments, and in turn affect subsequent treatment assignment and outcomes. This dynamic dependence complicates both causal identification and estimation.

Existing studies approach this problem from two directions: treatment-model-based and outcome-model-based. *Treatment-model-based* method, such as IPTW [22, 40, 49, 51, 56], aim to model treatment assignment to create a pseudo-population balanced on confounders. These methods often suffer from progressively increasing variance due to the multiplicative accumulation of propensity scores. *Outcome-model-based*, instead, tries to directly model the dynamics of the outcome. Among these methods, *Iterative Conditional Expectation (ICE) G-computation* has emerged as a prevalent approach. By breaking the problem into a series of conditional mean outcomes backward in time, ICE G-computation provides a stable alternative [28, 44, 47, 66]. However, its practical efficacy hinges on accurately modeling complex, high-dimensional relationships between time-varying confounders, treatments, and outcomes—a task where traditional parametric models often fail. This limitation has driven the adoption of **deep learning**, whose flexible function approximators (e.g., in DeepACE [17], GST-UNet [43], G-Transformer [23]) are well-suited to these complexities. Recent advances have productively merged this flexibility with the robustness of *doubly robust estimation*, as seen in Deep LTMLE [57], to hedge against model misspecification.

This deep learning implementation introduces a critical new challenge: autoregressive error propagation within a shared representation. Unlike traditional ICE, which fits independent regressions at each step, deep ICE trains one model whose predictions are recursively fed back as targets. Small errors in early steps compound into large biases for later ones, corrupting the training signal. This forces the model’s shared feature representation to adapt to increasingly erroneous pseudo-outcomes, a form of representation drift that undermines the stability of ICE and the robustness guarantees of DR estimation in finite samples.

In this work, we address deep ICE-specific instabilities through a novel **doubly debiased framework** that synergizes causal doubly robust estimation with architectural stabilization. Our approach, **D³-Net**, proceeds in two key stages: First, we integrate Sequential Doubly Robust (SDR) pseudo-outcomes into the ICE objective [37]. This mitigates error propagation in the recursive training of nuisance models by providing bias-corrected regression targets at each time step. To further stabilize learning, we employ a multi-task Transformer architecture augmented with a covariate simulator head and a target network. Second, we discard the SDR outputs after training and perform a final, optimal debiasing by applying Longitudinal Targeted Minimum Loss-Based Estimation (LTMLE)

to the original improved nuisance models. This combination secures both stable learning and robust inference. To summarize, our primary contributions are:

- **A bias-corrected ICE G-computation objective** that incorporates SDR pseudo-outcomes to reduce error propagation during the recursive training of outcome regressions. We show that this procedure provably mitigates error propagation in Lemma 4, thereby benefiting downstream inference.
- **A novel multi-task Transformer architecture** for longitudinal data that jointly learns treatment, outcome, and covariate simulation models. It employs a **target network** to smooth the moving targets and a **covariate simulator** for auxiliary supervision, together ensuring stable and accurate nuisance estimation.
- **A two-stage debiasing estimation procedure** that leverages the improved nuisances for LTMLE, yielding final estimates that are both robust and statistically efficient.
- **Comprehensive empirical validation** demonstrating that our framework, D^3 -Net, robustly achieves lower bias and variance than existing state-of-the-art longitudinal effect estimators.

2 Related work

Our work relates to longitudinal causal inference and off-policy evaluation (OPE) in reinforcement learning (RL), which share a core methodological challenge: estimating the value of a policy or treatment regime from observational data. Both confront analogous trade-offs among bias, variance, and stability when adjusting for time-varying confounding, yet have largely evolved in parallel.

Longitudinal Causal Estimation. Methods for estimating longitudinal effects are traditionally categorized by their reliance on treatment, outcome, or both models. Classic *treatment-model-based methods* use *Inverse Probability of Treatment Weighting* (IPTW) [11, 22, 49, 51, 52], its stabilized variant [8, 70], or matching [2, 61] to create balanced pseudo-populations. Recent deep learning methods adopted this principle and learn latent representations that predict outcomes while achieving a balance between treatment arms. Examples include RMSN [34], CRN [5], TE-CED [56], and Causal-Transformer [40]. These algorithms often perform poorly with finite samples in long horizons due to the compounding of small model errors in the treatment models, leading to high variance or residual bias [5, 11, 45].

The *outcome-model-based methods* paradigm directly models the outcome-generating process to estimate treatment effects using the *G-computation* [47, 58] by standardizing over the natural course of confounder distributions. Forward G-computation [9, 32, 39, 46, 63] simulates the time-varying confounder and outcomes based on the counterfactual treatments. While they often yield smaller variance [18], the need for a high-quality simulator is challenging in the finite-sample setting of healthcare. Recently, ICE G-computation gained attention due to the improved stability from its recursive formulation. It decomposes the problem into a sequence of conditional expectation estimations (i.e. step-wise Q -function estimation), thereby avoiding extensive Monte Carlo rollouts and reducing the accumulation of simulation errors in predicting time-varying covariates across long horizons. Examples include [17, 18, 36, 43].

Doubly robust methods, combining treatment and outcome models, enhance robustness against model misspecification, improving

finite-sample performance in high-dimensional, long-horizon settings. These include DML [6, 30], LTMLE [12, 17, 18, 20, 23, 53, 57, 59, 67] and SDR [12, 37]. Our work draws on recent SDR advances to augment the ICE G-computation objective, but then adopts LTMLE for the final estimation.

Off-Policy Evaluation in RL. OPE aims to estimate the value of a target policy using data collected from a different behavior policy, sharing a core statistical structure with longitudinal causal estimation. Methodologically, OPE approaches mirror the standard categories in longitudinal causal estimation and face the same core challenges: 1) *importance sampling* [21, 38, 55, 64], which reweights entire trajectories, corresponds to IPTW and suffers from the same extreme variance over long horizons [35]. 2) *Direct methods* (analogous to G-computation) model system dynamics to simulate counterfactual trajectories [13, 29, 68]. 3) *DR methods* improve finite-sample efficiency and retains consistency when either component is correctly specified [4, 14, 25, 27, 65].

Deep Learning for Sequential Estimation. Within the ICE G computation family, recent deep learning approaches exploit parameter sharing over time by using a single autoregressive model (e.g., LSTMs or Transformers) to estimate Q_t [17, 43, 57]. This design amortizes representation learning across steps while retaining the step-wise definition for Q_t . However, operating within the recursive structure in ICE, this sharing induces a ‘moving-target’ phenomenon that is well known in deep RL [19, 33, 41]. A standard remedy is the *target network*, a slowly updated copy of the major network is used to generate regression targets. Additionally, as the horizon grows, early-step targets in ICE G-computation can become increasingly noisy due to compounding approximation errors, motivating auxiliary supervision to regularize representations and improve learning from weak or noisy signals [16, 24, 60].

Our work is situated at the intersection of these fields. We focus on the deep learning implementation of the theoretically sound ICE G-computation framework. Inspired by stabilization techniques from deep RL, we employ a target network to smooth the recursive learning process and use auxiliary supervision to regularize representation learning. Furthermore, we uniquely combine the SDR transformation (to reduce error propagation in nuisance models) with a final LTMLE step (to ensure statistical robustness), creating a novel two-stage debiasing procedure tailored for stable and efficient deep longitudinal estimation.

3 Problem Setup and Preliminary

We consider n i.i.d longitudinal samples, each observed over τ discrete time steps and generated under an unknown treatment regime. For each time point $t \in \{1, \dots, \tau\}$, we observe time-varying covariates L_t , followed by a binary treatment assignment $A_t \in \mathcal{A} = \{0, 1\}$. A terminal outcome Y is observed after the final time point τ . Accordingly, the observed data for a single unit can be written as

$$O = (L_1, A_1, L_2, A_2, \dots, L_\tau, A_\tau, Y) \sim P_0,$$

where P_0 denotes the unknown true data-generating distribution. Any intermediate outcome observed after A_t can be absorbed into L_{t+1} without loss of generality.

For notational convenience, we use subscripts to represent temporal sequences, e.g., $X_{t:\tau} = (X_t, X_{t+1}, \dots, X_\tau)$. The information

available just before assigning treatment at time t is summarized by the history $H_t = \{L_i, A_i\}_{i=1}^{t-1} \cup \{L_t\} \in \mathcal{H}_t$. Both covariates and treatments may depend on the entire preceding history: L_t can be influenced by $H_{t-1} \cup \{A_{t-1}\}$, while treatment assignment at time t follows an unknown mechanism characterized by

$$G_t(H_t) = P(A_t = 1 | H_t), \quad (1)$$

where $G_t : \mathcal{H}_t \rightarrow (0, 1)$ denotes the propensity of receiving treatment conditional on the observed history.

Problem Setup. We aim to estimate the potential outcome of a counterfactual treatment sequence, such that decisions can be informed by comparing the potential outcomes of different sequences. Let $\mathbf{a} = (a_1, \dots, a_\tau)$ denote a generic counterfactual treatment sequence, and $Y(\mathbf{a})$ be the corresponding potential outcome. The **conditional average potential outcome (CAPO)** for sequence \mathbf{a} given baseline covariates L_1 is defined as $\psi = \mathbb{E}[Y(\mathbf{a})|L_1]$.

Throughout, we assume the standard longitudinal causal inference conditions to ensure the identifiability of our target parameters [17]: (1) Consistency: $Y(\mathbf{a}) = Y$ when $A_{1:\tau} = \mathbf{a}$; (2) Sequential Ignorability: $Y(\mathbf{a}) \perp A_t | H_t \quad \forall t \in \{1, \dots, \tau\}$; (3) Positivity: $\forall t \in \{1, \dots, \tau\}, P(A_t = a_t | H_t) > 0$.

The rest of the section reviews three key methodological building blocks. We first describe ICE G-computation (Sec. 3.1), which constructs plug-in estimates of longitudinal treatment effects. We then briefly review semi-parametric efficiency theory (Sec. 3.2). Grounded on the theory, we review LTMLE (Sec. 3.3) and SDR estimator (Sec. 3.4). They are both debiasing procedures that correct the first-order plug-in bias of initial estimators, including those from ICE, but differ in when the debiasing happens.

3.1 ICE G-computation

CAPO can be identified by the G-computation formula, which is a nested sequence of conditional expectations, evaluated under the counterfactual sequence \mathbf{a} [3, 48]:

$$\psi = \mathbb{E}\left[\mathbb{E}\left[\dots \mathbb{E}[Y|A_\tau = a_\tau, H_\tau] \dots\right] | A_2 = a_2, H_2\right] | A_1 = a_1, L_1]. \quad (2)$$

ICE G-computation estimates this quantity by breaking down the nested expectation into a series of recursive regression problems, proceeding backward from $t = \tau$ to $t = 1$. Define $Q_{\tau+1} = Y$. For each step $t = \tau, \dots, 1$, ICE G-computation recursively defines

$$Q_t(A_t, H_t) = \mathbb{E}[Q_{t+1}(a_{t+1}, H_{t+1}) | A_t, H_t]. \quad (3)$$

The CAPO is then identified as $\psi = \mathbb{E}[Q_1(a_1, H_1)]$.

Eq (3) implies that Q_t can be learned by regressing on the conditional expectation of $Q_{t+1}(a_{t+1}, H_{t+1})$, in the same spirit as temporal-difference learning in RL [62]. In practice, the expectation is not computed explicitly. Instead, the realized value $Q_{t+1}(a_{t+1}, H_{t+1})$ is directly used as the regression target for Q_t [17, 43, 57]. This can be viewed as a one-sample Monte Carlo estimate of the conditional expectation. While these targets are noisy, minimizing the regression loss with such targets at the population level recovers the desired conditional expectation.

Putting these together, ICE G-computation is implemented by iterating the following two steps from $t = \tau$ to 1:

- (1) Generate the regression target for step t by computing the realized value at step $t + 1$ under counterfactual treatment, $\hat{Q}_{t+1}(a_{t+1}, h_{t+1})$, a one-sample Monte Carlo simulation for the

expectation in Eq. (3). (At $t = \tau$, this step is skipped because the target is $\hat{Q}_{\tau+1} = Y$ by construction.)

- (2) Regress $Q_t(A_t, H_t)$ on the target $\hat{Q}_{t+1}(a_{t+1}, h_{t+1})$.

The estimate of ψ is obtained by averaging $\hat{Q}_1(a_1, h_1)$ over samples.

Remark 1. The pseudo-outcome at each step is conditioned on the observed history h_{t+1} , not the history altered by \mathbf{a} . While this may appear counterintuitive, the pseudo-outcome represents the conditional mean outcome given current history, under the intervention that follows \mathbf{a} from $t + 1$ onward. Under the standard assumptions, this conditional expectation is identifiable from the observed data.

While ICE G-computation provides a plug-in estimator that is consistent under correct model specification, its theoretical guarantees become difficult to maintain when using highly flexible function approximators such as transformers, which may overfit or introduce regularization bias. This limitation motivates doubly robust alternatives that explicitly correct estimation bias.

3.2 Semi-parametric Efficiency

Unlike ICE G-computation, which relies solely on outcome regression, doubly robust methods explicitly leverage the treatment model to correct bias so that the estimator is consistent even when one of the nuisance models (outcome or treatment) is misspecified. Here, we review the semi-parametric efficiency theory before introducing the DR methods, including LTMLE and SDR.

Let the target parameter $\psi = \Psi(P)$ be a functional of the data-generating distribution P . In practice, $\Psi(P)$ depends on nuisance components – in our case, the propensity score and outcome model at each time step. A plug-in estimator $\Psi(\hat{P})$ is obtained by substituting estimates of these nuisances. The error of this estimator can be expanded via a von Mises expansion [10, 67]:

$$\begin{aligned} \hat{\psi}_n - \psi_0 &= \mathbb{P}_n D_\Psi^*(P_0) - \underbrace{\mathbb{P}_n D_\Psi^*(\hat{P}_n)}_{\text{plug-in bias}} + \\ &\quad (\mathbb{P}_n - P_0)[D_\Psi^*(\hat{P}_n) - D_\Psi^*(P_0)] + R_2(\hat{P}_n, P_0), \end{aligned} \quad (4)$$

where $D_\Psi^*(P)$ is the influence function (IF) of ψ for the target parameter ψ under the nonparametric model for the data distribution P . Meanwhile, \mathbb{P}_n, P_0 are the empirical and true expectation operators, respectively; At a high level, all DR methods, despite their different approaches, aim to achieve asymptotic efficiency by eliminating the *plug-in bias term*, while relying on the remaining two terms to be $o_p(n^{-1/2})$ under regularity conditions [7, 67].

3.3 LTMLE

For our target estimand CAPO, its IF depends on the entire sequence of nuisance, $\{Q_t, G_t\}_{t=1}^\tau$ (defined in Eq. (1) and (3)):

$$D_\Psi^*(P)(O) = \sum_{s=1}^\tau \left\{ \left(\prod_{k=1}^s w_k \right) [Q_{s+1}(a_{s+1}, H_{s+1}) - Q_s(A_s, H_s)] \right\}, \quad (5)$$

where w_t is the inverse propensity score at time t

$$w_k = \frac{\mathbb{1}(A_k = a_k)}{a_k \cdot G_k(H_k) + (1 - a_k)(1 - G_k(H_k))} \quad (6)$$

Guided by the IF, LTMLE eliminates the plug-in bias term by iteratively updating the initial estimates of $\{Q_t\}_{t=1}^\tau$, so as to solve

Algorithm 1 SDR [12]

```

1: Input: Dataset  $\{O_i\}_{i=1}^n$ ; Initial estimates of  $G_t$  for  $t = 1, \dots, \tau$ 
2: Initialize  $Q_{\tau+1}^\dagger = Y$ 
3:
4: for  $t = \tau$  to 1 do
5:   (Learn) Use observed data to regress  $Q_t(A_t, H_t)$  on  $Q_{t+1}^\dagger(a_{t+1}, H_{t+1})$ 
6:   (Predict) Generate the regression target for  $Q_{t-1}(A_{t-1}, H_{t-1})$ 

$$Q_t^\dagger(a_t, h_t) = Q_t(a_t, h_t) + \sum_{s=t}^{\tau} \left\{ \left( \prod_{k=t}^s w_k \right) [Q_{s+1}(a_{s+1}, H_{s+1}) - Q_s(A_s, H_s)] \right\}. \quad (7)$$

7: end for
8: Final estimate  $\hat{\psi}_n = \mathbb{P}_n Q_1^\dagger(a_1, H_1)$ 

```

the score equation $\mathbb{P}_n D_\Psi^*(\hat{P}_n) = 0$. We refer readers to prior work [10, 31, 57, 67] for a detailed description of this procedure and Appendix A.1 for our implementations.

Let Q_t^0 and G_t^0 denote the true outcome and propensity score model, and \hat{Q}_t , \hat{G}_t their estimates. After the debiasing step, LTMLE provides the following multiply robust consistency:

Lemma 2 ($\tau+1$ multiply robust consistency of LTMLE [12]). Assume that there is a time k such that $\|\hat{Q}_t - Q_t^0\| = o_p(1)$ for all $t > k$ and $\|\hat{G}_t - G_t^0\| = o_p(1)$ for all $t \leq k$. Then we have $\hat{\psi}^d = \psi^d + o_p(1)$.

This result implies that consistency is achieved as long as all outcome regressions after some time point k are consistent and all propensity score models at and before k are consistent. For the τ -step-ahead CAPO, that indicate $\tau+1$ chances to obtain a consistent estimate. This condition is substantially weaker than those required by pure IPTW or G-computation, which require consistency of all propensity scores or all outcome regressions, respectively.

This robustness structure reflects when LTMLE applies debiasing. In particular, LTMLE first estimates the entire sequence of outcome regressions $\{Q_t\}_{t=1}^\tau$ via ICE G-computation, and then applies the IF-guided correction at the end. Consequently, the success of the debiasing step depends on the quality of the entire initial estimate of outcome models. Because ICE G-computation proceeds recursively backward in time, a poor estimate at some time k necessarily contaminates all downstream regressions Q_t for $t < k$, limiting the effectiveness of post-hoc debiasing.

3.4 SDR

The post-hoc debiasing strategy of LTMLE, while effective, is still not optimal. Recent developments in semi-parametric theory show that stronger robustness guarantees can be achieved. In particular, SDR estimators (see Algorithm 1) achieve consistency under substantially weaker conditions by requiring that, at each time step, *either* the outcome regression or the propensity score model be consistently estimated, leading to 2^τ chances to achieve consistency:

Lemma 3 (2^τ multiply robust consistency [12]). Assume that, for each time t , either $\|\hat{Q}_t - Q_t^\dagger\| = o_p(1)$ or $\|\hat{G}_t - G_t^0\| = o_p(1)$. Then we have $\hat{\psi}^d = \psi^d + o_p(1)$.

The fundamental difference between SDR and ICE G-computation lies in the regression target. Rather than regressing Q_t on the plug-in pseudo-outcome $\hat{Q}_{t+1}(a_{t+1}, H_{t+1})$, SDR regresses on a debiased target, $Q_{t+1}^\dagger(a_{t+1}, H_{t+1})$, that augments the plug-in estimate with an IF-based correction, as shown in Eq. (7) in Alg. 1. This leads to a crucial difference in the required consistency conditions: LTMLE relies on consistent estimation of the true model Q_t^0 (Lemma 2), whereas SDR only requires consistency between \hat{Q}_t and its constructed regression target Q_{t+1}^\dagger . As a result, SDR shifts the burden from accurately recovering the true outcome model to accurately fitting a regression, yielding a weaker requirement in finite samples.

To see the intention behind SDR, note that the augmentation term in Eq. (7) shares the same functional form as the IF in Eq. (5). This is not a coincidence: both are derived from solving the score equation for CAPO, differing only in the time point at which this statistical estimation problem is anchored. ICE G-computation identifies the final τ -step-ahead CAPO, $\mathbb{E}[Q_1(a_1, H_1)]$, by recursively modeling outcomes from the final time point backward. In contrast, the SDR transformation treats each intermediate quantity $\mathbb{E}[Q_t(a_t, H_t)]$ as a $(\tau - t)$ -step-ahead CAPO in its own right. Consequently, the augmentation term at step t is precisely the IF for that shorter-horizon estimand, thereby embedding local double robustness into the sequential regression updates.

Formally, at time t , the influence function for the $(\tau - t)$ -step-ahead CAPO is given by

$$D_\Psi^*(P)(O) = \sum_{s=t}^{\tau} \left\{ \left(\prod_{k=t}^s w_k \right) [Q_{s+1}(a_{s+1}, H_{s+1}) - Q_s(A_s, H_s)] \right\},$$

matching the augmentation term in Eq. (7). This construction is directly analogous to AIPTW for static CATE estimation, where debiasing is achieved by an additive IF correction [50, 54].

Although both LTMLE and SDR are multiply robust and rooted in the same semi-parametric efficiency theory, the key distinction between them lies in **when and how debiasing is applied**. LTMLE first fits the entire sequence of outcome regressions using ICE G-computation and then performs a *single, final debiasing step*, enforcing the score equation only for the τ -step-ahead CAPO. As a result, estimation errors may accumulate during the backward recursion before they are corrected.

In contrast, SDR *debiases recursively at every time step*. It treats each intermediate regression Q_t as a shorter-horizon CAPO estimand and enforces its corresponding score equation immediately. This stepwise fitting and debiasing prevents upstream errors from propagating downstream, yielding *sequential double robustness* throughout the estimation process. However, because its debiasing procedure directly incorporates a product of inverse propensity scores in the objective function at each step, it is susceptible to extreme weights and high variance in finite samples, particularly when propensity estimates are near the boundaries.

LTMLE does not exhibit this unstable behavior. Its debiasing is performed through a fluctuation of the outcome model within a parametric submodel, which ensures that the updated estimate naturally respects the support of the outcome and avoids the explosive variance associated with propensity score products. This tension, between SDR's recursive protection against error propagation and its potential for variance inflation, motivates our hybrid approach.

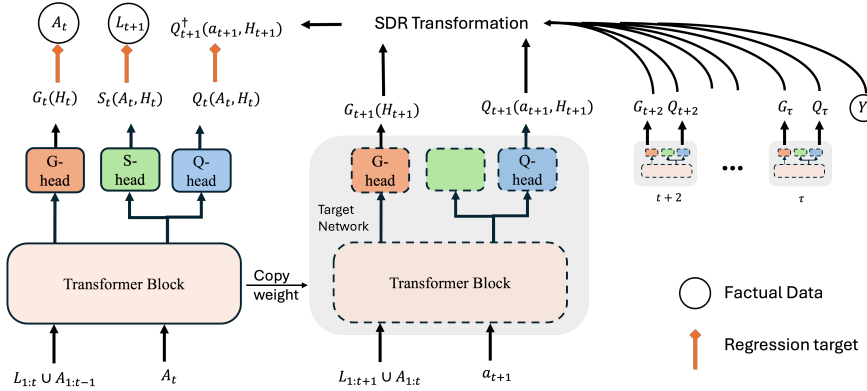


Figure 1: Overview of the D^3 -Net architecture and training procedure. D^3 -Net uses a shared multi-task Transformer backbone with the outcome (Q), treatment (G), and simulator (S) heads. At each time step t , the Q -head is trained using regression targets constructed from the SDR transformation, which combines future outcome and treatment models to form bias-corrected pseudo-outcomes $Q_{t+1}^\dagger(a_{t+1}, H_{t+1})$. A target network, implemented as a delayed copy of the main network, is used to generate stable SDR targets for recursive learning.

4 Methods

Our method consists of two stages: training and inference. During training, we use an SDR-augmented objective to embed debiasing into outcome regression and stabilize optimization with a target network (Section 4.1); we additionally regularize representation learning through auxiliary supervisions based on time-varying covariate prediction, and present the overall model architecture in Section 4.2. In the inference stage, we discard the SDR debiasing term and instead apply a final LTMLE targeting step, combining the strengths of both SDR and LTMLE; the resulting inference procedure and overall algorithm are described in Section 4.3.

4.1 Debias During Training via SDR

We first describe the training objective that integrates SDR-style debiasing into outcome regression. At a high level, we parameterize a sequence of outcome and treatment models $\{Q_t, G_t\}_{t=1}^\tau$, where Q_t are trained with supervision defined in SDR and G_t are supervised by factual treatment assignments.

Concretely, for each time step t , we construct an debiased pseudo-outcome $\hat{Q}_{t+1}^\dagger(a_{t+1}, H_{t+1})$ following Eq. (7). The Q -function is then trained by minimizing

$$\mathcal{L}_Q = \sum_{t=1}^\tau \mathbb{E} \left[(Q_t(A_t, H_t) - \hat{Q}_{t+1}^\dagger(a_{t+1}, H_{t+1}))^2 \right].$$

Analogous to the discussion of ICE (Section 3.1), this objective treats the realized value of $\hat{Q}_{t+1}^\dagger(a_{t+1}, H_{t+1})$ as a one sample Monte Carlo simulation for $\mathbb{E}[\hat{Q}_{t+1}^\dagger(a_{t+1}, H_{t+1})|A_t, H_t]$. Minimizing this at the population level recovers the SDR-defined supervision: $\hat{Q}_{t+1}^\dagger(a_{t+1}, H_{t+1}) = \mathbb{E}[\hat{Q}_{t+1}^\dagger(a_{t+1}, H_{t+1})|A_t, H_t]$. Meanwhile, the G -function is trained by minimizing $\sum_{t=1}^\tau L_{bce}(A_t, G_t(H_t))$, where $L_{bce}(x, \hat{x}) = x \log(\hat{x}) + (1 - x) \log(1 - \hat{x})$.

We parametrize $\{Q_t\}_{t=1}^\tau$ using a single, shared neural network. This allows the model to exploit the temporal structure in data, improving sample efficiency. However, in the recursive training of ICE or SDR, this shared parameterization introduces a **moving-target**:

at each iteration, Q_t is trained to regress on a pseudo-outcome \hat{Q}_{t+1}^\dagger that is itself produced by the same, changing parameters. After each gradient step, these shared parameters are updated, causing the regression target to shift, which leads to unstable training dynamics. The SDR augmentation compounds this issue, as its debiasing term involves a product of propensity scores that can introduce additional variance and amplify target fluctuations.

To stabilize training, we employ two techniques. First, we incorporate a *target network*, a standard heuristic from deep reinforcement learning. We maintain a slowly updated copy of the parameters via Polyak averaging (line 22, Algorithm 2) and use this lagged copy to compute the pseudo-outcome \hat{Q}_{t+1}^\dagger for the regression loss. This decouples the target from immediate parameter updates, smoothing its evolution across training iterations. Second, to maintain numerical stability, we address the fact that the SDR debiasing term can produce regression targets outside the natural outcome range. Since outcomes are min-max scaled to $[0, 1]$, we clip $\hat{Q}_{t+1}^\dagger(a_{t+1}, H_{t+1})$ to this interval before computing the loss, preventing extreme values from destabilizing training.

4.2 Auxiliary Supervision

To further improve representation learning, we introduce auxiliary tasks of next-step time-varying covariate prediction, which serve as a regularizer for learning informative longitudinal representations.

In longitudinal settings, the time-varying covariates L_t evolve according to complex dynamics that depend on past covariates and treatments. Capturing such dynamics is critical for accurate outcome and treatment modeling. However, supervision from outcome regression alone is limited, as it is mediated only through the terminal outcome signal. While the commonly fitted treatment model provides additional supervision, it still does not fully constrain the representation to encode the temporal dynamics.

To enrich the training signal and regularize representation learning, we begin by introducing an auxiliary prediction task that explicitly models covariate dynamics. In addition to the Q - and G -functions discussed in Section 4.1, we augment the architecture

with an auxiliary simulator (the S -function) that predicts next-step covariates given the current history and treatment. The auxiliary objective is defined as $\mathcal{L}_S = \sum_{t=1}^{\tau} (S_t(A_t, H_t) - L_{t+1})^2$. This auxiliary supervision encourages the shared representation to encode information relevant to the temporal evolution of the patient state, thereby improving generalization of the learned features.

Note that the treatment model G_t , which predicts A_t given $(L_{1:t}, A_{1:t-1})$, together with the auxiliary simulator S_t , which predicts L_{t+1} given $(L_{1:t}, A_{1:t})$, effectively implements a next-step (next-token) prediction structure that captures the entire input sequence. Although our formulation adopts a simplified view in which all covariates at time t are summarized into L_t , this abstraction can be readily extended to more general settings where L_t itself contains temporally ordered observations.

Combining these components, our model architecture is shown in Figure 1. The backbone is adapted from the heterogeneous Transformer in DeepLTMLE [57]. Inputs are first passed through a type-embedding layer distinguishing covariates L , treatment A , and outcome Y , and combined with positional encodings. The resulting embedding is processed by a Transformer block, whose output feeds into a Q -head for outcome regression, a G -head for treatment prediction, and an S -head for covariate prediction. All ‘heads’ are a linear layer followed by an activation function. Q uses sigmoid activation as the outcome is bounded between 0 and 1;¹ G uses sigmoid as the treatment is binary; S uses none, as the covariates in our experiments are all continuous.

The Q function, G , and S functions are evaluated at different time steps through their respective time-specific inputs. At step t , G_t have access to H_t , S_t and Q have access to (H_t, A_t) . This is enforced by masking future variables in the input sequence.

4.3 Re-debias via LTMLE

As discussed in Section 3.4 SDR may suffer from large variance due to the product of inverse propensity scores. Although we use hard clipping of the pseudo-outcome to improve the numeric stability of training, we recognize that such hard clipping risks introducing bias. Therefore, we propose a hybrid strategy: after training, we drop the SDR correction terms and treat the uncorrected outcome models, $\hat{Q}_t(a_t, H_t)$, as estimated nuisance and perform LTMLE (line 27-34 in Algorithm 2; LTMLE are detailed in Algorithm A.1). Intuitively, training under SDR improves the quality of the initial Q -functions, while LTMLE provides finite-sample stability. The following lemma characterizes how the training targets induce either first-order (ICE) or second-order (SDR) dependence on upstream nuisance errors, clarifying why SDR initialization can yield better initial outcome regressions for subsequent LTMLE targeting (Proof in Appendix B).

Lemma 4 (First- vs. second-order dependence in training targets). Assume bounded outcomes and positivity. Let \hat{Q}_t^{ICE} be the initial estimate from regular ICE G-computation, and let \hat{Q}_t^{SDR} be the initial estimate from SDR procedure. Throughout, we suppress function arguments when clear from context; e.g., Q_t^0 denotes $Q_t^0(A_t, H_t)$ and G_k^0 denotes $G_k^0(A_k | H_k)$ unless arguments are shown explicitly.

¹While Q uses sigmoid activation, the corresponding objective is an MSE loss between the sigmoid-bounded Q and the pseudo-outcome.

Algorithm 2 D^3 -Net

```

1: Training:
2: Input: Training data  $\{O_i\}_{i=1}^n$ ; horizon  $\tau$ ; target network update rate  $\beta$ .
3: Initialize  $\theta$ ; set target copy  $\theta' \leftarrow \theta$ .
4: for batch = 1, ...,  $B$  do
5:   (Major model forward) For  $t = 1, \dots, \tau$ :
6:      $Q_t(A_t, H_t) \leftarrow h_Q(\phi(H_t, A_t; \theta_\phi); \theta_Q)$ 
7:      $G_t(H_t) \leftarrow h_G(\phi(H_t; \theta_\phi); \theta_G)$ 
8:      $S_t(A_t, H_t) \leftarrow h_S(\phi(H_t, A_t; \theta_\phi); \theta_S)$ 
9:   (Target network forward for SDR) For  $t = 1, \dots, \tau$ :
10:     $Q'_t(A_t, H_t) \leftarrow h_Q(\phi(H_t, A_t; \theta'_\phi); \theta'_Q)$ 
11:     $Q'_t(a_t, H_t) \leftarrow h_Q(\phi(H_t, a_t; \theta'_\phi); \theta'_Q)$ 
12:     $G'_t(H_t) \leftarrow h_G(\phi(H_t; \theta'_\phi); \theta'_G)$ 
13:     $Q_{t+1}^\dagger \leftarrow Y$ 
14:   for  $t = \tau, \dots, 1$  do
15:     Compute  $Q_{t+1}^\dagger(a_{t+1}, H_{t+1})$  via SDR transformation (Eq. (7))
         using  $\{Q'_s(\cdot), G'_s(\cdot)\}_{s=t+1}^\tau$ .
16:   end for
17:    $\mathcal{L}_Q \leftarrow \sum_{t=1}^{\tau} (Q_t(A_t, H_t) - Q_{t+1}^\dagger(a_{t+1}, H_{t+1}))^2$ 
18:    $\mathcal{L}_G \leftarrow \sum_{t=1}^{\tau} L_{\text{bce}}(A_t, G_t(H_t))$ 
19:    $\mathcal{L}_S \leftarrow \sum_{t=1}^{\tau} (S_t(A_t, H_t) - L_{t+1})^2$ 
20:    $\mathcal{L} \leftarrow \mathcal{L}_Q + \alpha(\mathcal{L}_G + \mathcal{L}_S)$ 
21:    $\theta \leftarrow \theta - \eta \nabla_{\theta} \mathcal{L}$ 
22:    $\theta' \leftarrow \beta \theta + (1 - \beta) \theta'$ 
23: end for
24: Output: parameters  $\theta = (\theta_\phi, \theta_Q, \theta_G, \theta_S)$ .
25:
26: Inference:
27: Input: Evaluation Data  $\{O_i\}_{i=1}^m$ .
28: for  $t = 1, \dots, \tau$  do
29:    $G_t(H_t) = h_G(\phi(H_t; \theta_\phi); \theta)$ 
30:    $Q_t(A_t, H_t) = h_Q(\phi(H_t, A_t; \theta_\phi); \theta_Q)$ 
31: end for
32: Output:  $\hat{\psi} = \text{LTMLE}(\{O_i\}_{i=1}^m; \{Q_t\}_{t=1}^\tau; \{G_t\}_{t=1}^\tau)$ 

```

Then, for each $t = 1, \dots, \tau - 1$, the population regression errors admit the bounds

$$\begin{aligned} \|\hat{Q}_t^{\text{ICE}} - Q_t^0\|_2 &\leq \xi_t^{\text{ICE}} + \|\hat{Q}_{t+1}^{\text{ICE}}(a_{t+1}, H_{t+1}) - Q_{t+1}^0(a_{t+1}, H_{t+1})\|_2, \\ \|\hat{Q}_t^{\text{SDR}} - Q_t^0\|_2 &\leq \xi_t^{\text{SDR}} + \sum_{k=t+1}^{\tau} C_{t,k} \|\hat{G}_k^{\text{SDR}} - G_k^0\|_2 \|\hat{Q}_k^{\text{SDR}} - Q_k^\dagger\|_2, \end{aligned}$$

for constants $C_{t,k}$ depending only on positivity and τ , where ξ_t^{ICE} and ξ_t^{SDR} denotes the regression-to-target error at time t for corresponding estimator.

This lemma shows that, under regular ICE G-computation, the error in \hat{Q}_t^{ICE} exhibits first-order dependence on upstream outcome regression error. We note that $\|\hat{Q}_{t+1}^{\text{ICE}}(a_{t+1}, H_{t+1}) - Q_{t+1}^0(a_{t+1}, H_{t+1})\|_2$ is evaluated at (a_{t+1}, H_{t+1}) and thus this bound does not directly telescope into a horizon-wide inequality under the same shorthand norm. In contrast, using training targets debiased by SDR transformation yields a second-order dependence on upstream outcome and propensity-score estimation errors. Notably, the product doesn’t involve the next-step error to the true model ($\|\hat{Q}_k^{\text{SDR}} - Q_k^0\|_2$), but

involves the error to the constructed target ($\|\hat{Q}_k^{\text{SDR}} - Q_k^\dagger\|_2$). Consequently, the effect of upstream nuisance estimation enters only at second order, which makes the error propagation across time more amenable to control. D^3 -Net couples this improved nuisance estimation with LTMLE targeting, making the multiply robust consistency condition of LTMLE (Lemma 2) easier to satisfy in practice.

5 Experiments

We assess D^3 -Net using semi-synthetic benchmarks constructed from MIMIC-III [26], a real-world critical care dataset. Section 5.1 describes the experimental design. Building on the benchmarking configuration of DeepACE, we further evaluate our methods under stronger time-varying confoundings and various horizons. Section 5.2 reports quantitative results, where D^3 -Net demonstrates consistent lower bias and variance in these challenging settings. Section 5.3 present ablation studies.

5.1 Setup

Baselines. We benchmark D^3 -Net against ICE G-computation-based longitudinal estimators, including (1) G-computation with Super Learner (2) LTMLE with Super Learner, (3) DeepACE, and (4) DeepLTMLE. Together, these methods span a range of modeling expressiveness and debiasing strategies within this framework. Implementation details are provided in Appendix C.1.

Settings. We begin with the semi-synthetic DGP proposed in DeepACE, which combines 10 real time-varying clinical measurements from MIMIC-III with synthetically generated treatment assignments and outcomes. In this setting, treatment affects the single outcome variable but does not affect any other covariates, yielding a limited treatment-confounder feedback mechanism.

To study more challenging scenarios, we further augment this DGP with five additional synthetic time-varying covariates that both affect and are affected by treatment, thereby inducing an expanded and more realistic feedback structure. We refer to these two settings as *Limited Time-varying Confounding* and *Expanded Time-varying Confounding* throughout the paper. Full specifications of both DGPs are provided in Appendix C.2.

For each DGP, we sample $N = 1500$ patient trajectories and generate longitudinal data over different horizon lengths τ . We begin with $\tau = 15$, as chosen by DeepACE. Hyperparameter tuning procedures for all baselines are detailed in Appendix C.3.

Because longitudinal estimators can exhibit different bias behavior under different counterfactual treatments, we evaluate each method across multiple counterfactual treatment sequences rather than a single one. Similar to DeepACE, we evaluate four counterfactual sequences for each horizon: CF 1: never treat; CF 2: always treat; CF 3: treat in the first half of the horizon; CF 4: treat in the second half of the horizon (Details in Appendix C.4). All experiments are repeated over 20 random seeds for each method, horizon, and counterfactual setting. This yields 20 absolute bias values per setting, while a single RMSE is computed by aggregating errors across the 20 runs.

5.2 Results

Figure 2 summarizes performance by aggregating absolute bias across counterfactual sequences. Across all horizons and under

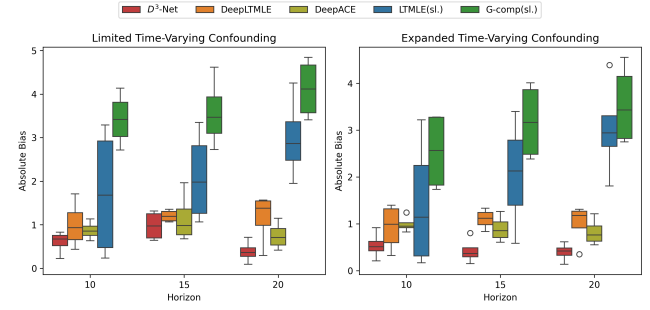


Figure 2: Absolute bias of CAPO estimates across counterfactual sequences for horizons $\tau \in 10, 15, 20$ under limited (left) and expanded (right) time-varying confounding. D^3 -Net consistently achieves lower bias and smaller dispersion.

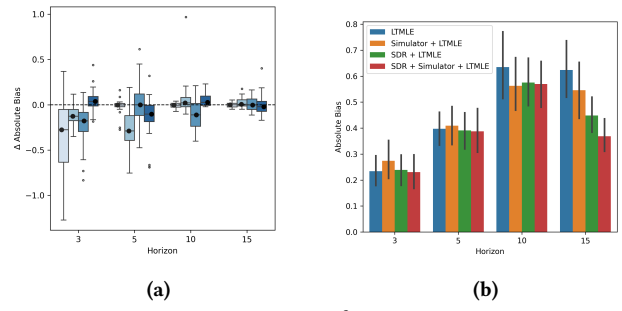


Figure 3: Ablation study of D^3 -Net. Left: Effect of LTMLE re-debiasing on top of SDR across horizons; the y-axis shows the change in absolute bias (LTMLE minus raw SDR), with each box corresponding to a counterfactual sequence. Right: Ablation of training components across horizons; the y-axis shows mean absolute bias \pm standard deviation.

both limited and expanded time-varying confounding, D^3 -Net consistently achieves lower error than all baselines, indicating strong overall performance. Tables 1, 2, and S1 report detailed results for each individual counterfactual sequence.²

Beyond average performance, a key strength of D^3 -Net is its **robustness across different settings**. While several baselines perform competitively for specific counterfactuals under limited confounding and short horizons, their performance degrades markedly as the horizon increases or the treatment-confounder feedback becomes stronger. In contrast, D^3 -Net consistently attains the lowest or second-lowest RMSE across all horizons, confounding settings, and counterfactual sequences, demonstrating robust performance. This stability is particularly pronounced in the more challenging settings with longer horizons and expanded confounding.

Notably, despite having a similar expressiveness as DeepLTMLE because both models use a transformer backbone, D^3 -Net yields substantial improvement. This gap highlights the benefit of training nuisances using the proposed SDR-debiased supervision together with auxiliary supervision. Overall, these results show that the advantages of D^3 -Net are not confined to a single policy or regime,

²In experiments, DeepACE diverges (1–3 out of 20 seeds), leading to extreme estimates. These runs are excluded from summary statistics and marked with * in the tables.

Table 1: Absolute bias (mean \pm std) and RMSE of CAPO estimates at horizon $\tau = 15$.

Model	Limited Time-varying Confounding								Expanded Time-varying Confounding							
	Bias				RMSE				Bias				RMSE			
	CF 1	CF 2	CF 3	CF 4	CF 1	CF 2	CF 3	CF 4	CF 1	CF 2	CF 3	CF 4	CF 1	CF 2	CF 3	CF 4
G-comp (sl.)	3.22 \pm 2.19	3.71 \pm 1.71	2.73 \pm 1.85	4.62 \pm 1.88	3.87	4.07	3.27	4.97	2.52 \pm 1.07	3.81 \pm 1.74	2.38 \pm 1.03	4.01 \pm 1.19	2.73	4.17	2.59	4.17
LTM. (sl.)	2.63 \pm 1.60	3.35 \pm 2.20	1.33 \pm 1.22	1.06 \pm 1.15	3.06	3.98	1.78	1.55	2.58 \pm 1.02	3.40 \pm 3.41	0.58 \pm 0.40	1.67 \pm 1.59	2.77	3.66	0.70	2.28
D.ACE	1.16 \pm 0.20	0.68\pm0.17	1.96 \pm 3.33*	0.8 \pm 0.34	1.17	0.70	3.78	0.87	1.27 \pm 0.15	<u>0.61\pm0.13</u>	0.96 \pm 0.99*	0.74 \pm 0.66	<u>1.27</u>	<u>0.62</u>	1.36	<u>0.98</u>
D.LTMLE	<u>1.10\pm0.76</u>	1.36 \pm 0.73	<u>1.07\pm0.36</u>	1.29 \pm 0.74	1.32	1.53	<u>1.12</u>	1.48	<u>1.03\pm1.22</u>	1.21 \pm 0.72	1.3 \pm 1.40	0.84 \pm 0.70	1.57	1.40	1.39	1.08
D^3 -Net	0.71\pm0.59	1.32 \pm 0.47	1.23 \pm 0.35	0.92	<u>1.39</u>	0.65	<u>1.28</u>	0.80\pm0.76	<u>0.34\pm0.25</u>	<u>0.38\pm0.21</u>	<u>0.15\pm0.11</u>	1.09	0.42	0.43	0.18	

Table 2: Absolute bias (mean \pm std) and RMSE of CAPO estimates at horizon $\tau = 20$.

Model	Limited Time-varying Confounding								Expanded Time-varying Confounding							
	Bias				RMSE				Bias				RMSE			
	CF 1	CF 2	CF 3	CF 4	CF 1	CF 2	CF 3	CF 4	CF 1	CF 2	CF 3	CF 4	CF 1	CF 2	CF 3	CF 4
G-comp (sl.)	3.41 \pm 1.05	4.61 \pm 1.21	3.63 \pm 1.33	4.84 \pm 1.30	3.56	4.75	3.85	5.00	2.75 \pm 1.37	4.01 \pm 1.43	2.85 \pm 1.18	4.55 \pm 1.15	3.06	4.25	3.07	4.69
LTM. (sl.)	3.07 \pm 1.41	4.25 \pm 1.30	1.95 \pm 1.65	2.66 \pm 1.53	3.37	4.44	2.53	3.05	2.93 \pm 1.28	4.39 \pm 1.47	1.83 \pm 1.30	2.95 \pm 1.36	3.19	4.62	2.21	3.23
D.ACE	1.15 \pm 0.15	0.57 \pm 0.10	0.84 \pm 0.42*	0.42 \pm 0.45	1.16	0.58	0.93	0.60	<u>1.21\pm0.11</u>	<u>0.65\pm0.08</u>	<u>0.87\pm0.40*</u>	<u>0.55 \pm 0.57</u>	1.22	0.66	0.95	0.79
D.LTMLE	1.22 \pm 0.94	1.54 \pm 0.78	<u>0.30\pm0.26</u>	1.57 \pm 1.55	1.52	1.72	<u>0.39</u>	2.18	1.31 \pm 1.20	1.10 \pm 0.66	<u>0.35\pm0.21</u>	1.25 \pm 1.20	1.75	1.28	<u>0.40</u>	1.71
D^3 -Net	0.71\pm0.48	0.33\pm0.23	0.09\pm0.08	0.39\pm0.36	0.85	0.40	0.12	0.52	0.61\pm0.48	0.44\pm0.34	0.14\pm0.08	0.39 \pm 0.31	0.77	0.55	0.16	0.50

but persist across horizons, confounding strengths, and counterfactual sequences, highlighting its robustness to error propagation and treatment-confounder feedback.

5.3 Ablation Study

Our method consists of a training and an inference stage. We first evaluate the impact of applying LTMLE at inference stage to re-debias the SDR-initialized nuisances, compared to using the raw SDR estimates. Then, with LTMLE enabled at inference, we ablate the training-stage components: SDR and auxiliary supervision.

Figure 3a shows that applying LTMLE to re-debias the SDR-initialized nuisances often reduces bias, with substantial improvements in several counterfactuals and horizons, while in a few cases it leads to negligible increases. This behavior highlights both the limitations of raw SDR and the role of LTMLE as a generally stabilizing correction step. While the gains become smaller at longer horizons, where both methods are challenged by near-violations of the positivity assumption, LTMLE does not degrade performance and thus serves as a safeguard.

Next, with LTMLE in place, we investigate the roles of SDR-debiasing and the simulator supervision across different horizons. Figure 3b and Figure S2 compare variants that selectively enable SDR and/or the simulator. Aggregated over counterfactual sequences, enabling SDR or simulator alone reduces bias at long horizons, while at shorter horizons, the effects are mixed and can be negligible. Enabling both yields only modest additional gains over enabling SDR alone, indicating that SDR is the primary driver of performance improvements. At the level of individual counterfactuals, the effect is heterogeneous, but the overall trend favors SDR, while adding the simulator on top of SDR yields smaller, setting-dependent changes that act as a complementary regularization.

5.4 Real-world Case Study

We applied D^3 -Net on a intensive care cohort derived from MIMIC-IV, focusing on patients with sepsis complicated by hypotension to study the effects of alternative vasopressor weaning strategies. The study population consists of 999 adult ICU patients who satisfied Sepsis-3 criteria, experienced hypotension ($MAP \leq 65$ mmHg), and received vasopressor within the first 24 hours after ICU admission.

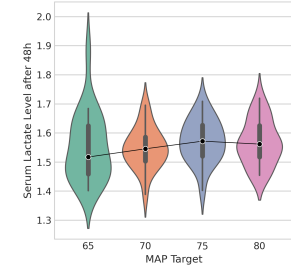


Figure 4: Distribution of CAPO estimates of 72-hour serum lactate across four MAP targets (65–80 mmHg), aggregated over 20 bootstrap experiments. Higher MAP targets are associated with modestly higher lactate levels, consistent with prior evidence and current clinical guidelines.

As the clinical endpoint, we considered serum lactate measured at 72 hours, which is widely used as an indicator of tissue hypoperfusion and disease severity in septic shock [42].

We examined four treatment regimes corresponding to discontinuing vasopressors once MAP had been sustained above 65, 70, 75, or 80 mmHg for a 12-hour window (Details in Appendix E). Figure 4 summarizes the resulting CAPO estimates of 20 Bootstrap experiments. Across these policies, we observe a pattern in which more aggressive MAP targets are associated with slightly higher lactate levels at 72 hours (higher lactate often implies worse outcome). This observation is consistent with prior randomized evidence showing no survival advantage from targeting higher MAP thresholds [1], and it is directionally aligned with current clinical guidelines that caution against unnecessary vasopressor exposure [15].

6 Conclusion

We propose D^3 -Net, a two-stage framework that integrates SDR-based training with LTMLE targeting, using a target network and simulator to stabilize and regularize deep ICE G-computation. Experiments demonstrate its robustness across settings.

7 GenAI Disclosure

We used generative AI tools only for language polishing and code debugging. All scientific ideas, methods, and experiments were developed and validated by the authors.

8 Limitations and Ethical Considerations

We use the publicly available, de-identified MIMIC-III and MIMIC-IV datasets in accordance with their data use policies, without any direct interaction with human subjects. As with all observational studies, our results rely on standard causal assumptions and may be affected by unmeasured confounding, so they should not be interpreted as direct clinical recommendations without further investigation.

Acknowledgments

We thank Lillian Li for her assistance with data preprocessing.

References

- [1] Pierre Asfar, Ferhat Meziani, Jean-François Hamel, Fabien Grelon, Bruno Megarbane, Nadia Anguel, Jean-Paul Mira, Pierre-François Dequin, Soizic Gergaud, Nicolas Weiss, et al. 2014. High versus low blood-pressure target in patients with septic shock. *New England Journal of Medicine* 370, 17 (2014), 1583–1593.
- [2] Peter C Austin. 2011. An introduction to propensity score methods for reducing the effects of confounding in observational studies. *Multivariate behavioral research* 46, 3 (2011), 399–424.
- [3] Heejung Bang and James M Robins. 2005. Doubly robust estimation in missing data and causal inference models. *Biometrics* 61, 4 (2005), 962–973.
- [4] Aurelien Bibaut, Ivana Malenica, Nikos Vlassis, and Mark Van Der Laan. 2019. More efficient off-policy evaluation through regularized targeted learning. In *International Conference on Machine Learning*. PMLR, 654–663.
- [5] Ioana Bica, Ahmed M Alaa, James Jordon, and Mihaela van der Schaar. 2020. Estimating counterfactual treatment outcomes over time through adversarially balanced representations. In *International Conference on Learning Representations*.
- [6] Hugo Bodory, Martin Huber, and Lukáš Lafférs. 2022. Evaluating (weighted) dynamic treatment effects by double machine learning. *The Econometrics Journal* 25, 3 (2022), 628–648.
- [7] Victor Chernozhukov, Denis Chetverikov, Mert Demirer, Esther Duflo, Christian Hansen, Whitney Newey, and James Robins. 2018. Double/debiased machine learning for treatment and structural parameters.
- [8] Nicholas C Chesnaye, Vianda S Stel, Giovanni Triepi, Friedo W Dekker, Edouard L Fu, Carmine Zoccali, and Kitty J Jager. 2022. An introduction to inverse probability of treatment weighting in observational research. *Clinical kidney journal* 15, 1 (2022), 14–20.
- [9] Yu-Han Chiu, Lan Wen, Sean McGrath, Roger Logan, Issa J Dahabreh, and Miguel A Hernán. 2023. Evaluating model specification when using the parametric g-formula in the presence of censoring. *American journal of epidemiology* 192, 11 (2023), 1887–1895.
- [10] Brian M Cho, Yaroslav Mukhin, Kyra Gan, and Ivana Malenica. 2024. Kernel Debiased Plug-in Estimation: Simultaneous, Automated Debiasing without Influence Functions for Many Target Parameters. In *International Conference on Machine Learning*. PMLR, 8534–8555.
- [11] Stephen R Cole and Miguel A Hernán. 2008. Constructing inverse probability weights for marginal structural models. *American journal of epidemiology* 168, 6 (2008), 656–664.
- [12] Iván Díaz, Nicholas Williams, Katherine L Hoffman, and Edward J Schenck. 2023. Nonparametric causal effects based on longitudinal modified treatment policies. *J. Amer. Statist. Assoc.* 118, 542 (2023), 846–857.
- [13] Yaqi Duan, Zeyu Jia, and Mengdi Wang. 2020. Minimax-optimal off-policy evaluation with linear function approximation. In *International Conference on Machine Learning*. PMLR, 2701–2709.
- [14] Miroslav Dudík, John Langford, and Lihong Li. 2011. Doubly Robust Policy Evaluation and Learning. *CoRR* abs/1103.4601 (2011). arXiv:1103.4601 <http://arxiv.org/abs/1103.4601>
- [15] Laura Evans, Andrew Rhodes, Waleed Alhazzani, Massimo Antonelli, Craig M Coopersmith, Craig French, Flávia R Machado, Lauralyn McIntyre, Marlies Ostermann, Hallie C Prescott, et al. 2021. Surviving sepsis campaign: international guidelines for management of sepsis and septic shock 2021. *Critical care medicine* 49, 11 (2021), e1063–e1143.
- [16] Ching Fang and Kimberly L Stachenfeld. 2023. Predictive auxiliary objectives in deep rl mimic learning in the brain. *arXiv preprint arXiv:2310.06089* (2023).
- [17] Dennis Frauen, Tobias Hatt, Valentyn Melnychuk, and Stefan Feuerriegel. 2023. Estimating average causal effects from patient trajectories. In *Proceedings of the AAAI Conference on Artificial Intelligence*, Vol. 37. 7586–7594.
- [18] Dennis Frauen, Konstantin Hess, and Stefan Feuerriegel. 2024. Model-agnostic meta-learners for estimating heterogeneous treatment effects over time. *arXiv preprint arXiv:2407.05287* (2024).
- [19] Justin Fu, Aviral Kumar, Matthew Soh, and Sergey Levine. 2019. Diagnosing bottlenecks in deep q-learning algorithms. In *International Conference on Machine Learning*. PMLR, 2021–2030.
- [20] Suhan Guo, Furao Shen, and Ni Li. 2024. Estimating the treatment effect over time under general interference through deep learner integrated TMLE. *arXiv preprint arXiv:2412.04799* (2024).
- [21] Josiah Hanna, Scott Niekuam, and Peter Stone. 2019. Importance sampling policy evaluation with an estimated behavior policy. In *International Conference on Machine Learning*. PMLR, 2605–2613.
- [22] Miguel A Hernán and James M Robins. 2006. Estimating causal effects from epidemiological data. *Journal of Epidemiology & Community Health* 60, 7 (2006), 578–586.
- [23] Konstantin Hess, Dennis Frauen, Valentyn Melnychuk, and Stefan Feuerriegel. 2024. G-transformer for conditional average potential outcome estimation over time. *arXiv preprint arXiv:2405.21012* (2024).
- [24] Max Jaderberg, Volodymyr Mnih, Wojciech Marian Czarnecki, Tom Schaul, Joel Z Leibo, David Silver, and Koray Kavukcuoglu. 2016. Reinforcement learning with unsupervised auxiliary tasks. *arXiv preprint arXiv:1611.05397* (2016).
- [25] Nan Jiang and Lihong Li. 2016. Doubly Robust Off-policy Value Evaluation for Reinforcement Learning. In *Proceedings of The 33rd International Conference on Machine Learning (Proceedings of Machine Learning Research, Vol. 48)*. Maria Florina Balcan and Kilian Q. Weinberger (Eds.). PMLR, New York, New York, USA, 652–661. <https://proceedings.mlr.press/v48/jiang16.html>
- [26] Alistair Johnson, Tom Pollard, and Roger Mark. 2016. MIMIC-III Clinical Database. *PhysioNet* (Sept. 2016). doi:10.13026/C2XW26 Version 1.4.
- [27] Nathan Kallus and Masatoshi Uehara. 2020. Double Reinforcement Learning for Efficient Off-Policy Evaluation in Markov Decision Processes. *Journal of Machine Learning Research* 21, 167 (2020), 1–63. <http://jmlr.org/papers/v21/19-827.html>
- [28] Alexander P Keil, Jessie K Edwards, David B Richardson, Ashley I Naimi, and Stephen R Cole. 2014. The parametric g-formula for time-to-event data: intuition and a worked example. *Epidemiology* 25, 6 (2014), 889–897.
- [29] Hoang Le, Cameron Voloshin, and Yisong Yue. 2019. Batch policy learning under constraints. In *International Conference on Machine Learning*. PMLR, 3703–3712.
- [30] Greg Lewis and Vasilis Syrgkanis. 2021. Double/Debiased Machine Learning for Dynamic Treatment Effects.. In *NeurIPS*. 22695–22707.
- [31] Diyang Li and Kyra Gan. 2025. Targeted Maximum Likelihood Learning: An Optimization Perspective. In *The Thirty-ninth Annual Conference on Neural Information Processing Systems*. <https://openreview.net/forum?id=n63KgrgVHG>
- [32] Rui Li, Stephanie Hu, Mingyu Lu, Yuria Utsumi, Prithwish Chakraborty, Daby M Sow, Piyush Madan, Jun Li, Mohamed Ghalwash, Zach Shah, et al. 2021. G-net: a recurrent network approach to g-computation for counterfactual prediction under a dynamic treatment regime. In *Machine Learning for Health*. PMLR, 282–299.
- [33] Timothy P Lillicrap, Jonathan J Hunt, Alexander Pritzel, Nicolas Heess, Tom Erez, Yuval Tassa, David Silver, and Daan Wierstra. 2015. Continuous control with deep reinforcement learning. *arXiv preprint arXiv:1509.02971* (2015).
- [34] Bryan Lim. 2018. Forecasting treatment responses over time using recurrent marginal structural networks. *Advances in neural information processing systems* 31 (2018).
- [35] Qiang Liu, Lihong Li, Ziyang Tang, and Dengyong Zhou. 2018. Breaking the curse of horizon: Infinite-horizon off-policy estimation. *Advances in neural information processing systems* 31 (2018).
- [36] Ruyi Liu, Liangyuan Hu, Francis Perry Wilson, Joshua L Warren, and Fan Li. 2025. A Bayesian Approach to the G-Formula via Iterative Conditional Regression. *Statistics in Medicine* 44, 13–14 (2025), e70123.
- [37] Alexander R Luedtke, Oleg Sofrygin, Mark J van der Laan, and Marco Carone. 2017. Sequential double robustness in right-censored longitudinal models. *arXiv preprint arXiv:1705.02459* (2017).
- [38] A Rupam Mahmood, Hado P Van Hasselt, and Richard S Sutton. 2014. Weighted importance sampling for off-policy learning with linear function approximation. *Advances in neural information processing systems* 27 (2014).
- [39] Sean McGrath, Victoria Lin, Zilu Zhang, Lucia C Petito, Roger W Logan, Miguel A Hernán, and Jessica G Young. 2020. gfoRmula: an R package for estimating the effects of sustained treatment strategies via the parametric g-formula. *Patterns* 1, 3 (2020).
- [40] Valentyn Melnychuk, Dennis Frauen, and Stefan Feuerriegel. 2022. Causal transformer for estimating counterfactual outcomes. In *International conference on machine learning*. PMLR, 15293–15329.
- [41] Volodymyr Mnih, Koray Kavukcuoglu, David Silver, Alex Graves, Ioannis Antonoglou, Daan Wierstra, and Martin Riedmiller. 2013. Playing atari with deep reinforcement learning. *arXiv preprint arXiv:1312.5602* (2013).

[42] H Bryant Nguyen, Manisha Loomba, James J Yang, Gordon Jacobsen, Kant Shah, Ronny M Otero, Arturo Suarez, Hemal Parekh, Anja Jaehne, and Emanuel P Rivers. 2010. Early lactate clearance is associated with biomarkers of inflammation, coagulation, apoptosis, organ dysfunction and mortality in severe sepsis and septic shock. *Journal of inflammation* 7, 1 (2010), 6.

[43] Miruna Oprisescu, David Keetae Park, Xihai Luo, Shinjae Yoo, and Nathan Kallus. 2025. GST-UNet: A Neural Framework for Spatiotemporal Causal Inference with Time-Varying Confounding. In *The Thirty-ninth Annual Conference on Neural Information Processing Systems*.

[44] Maya Petersen, Joshua Schwab, Susan Gruber, Nello Blaser, Michael Schomaker, and Mark van der Laan. 2014. Targeted maximum likelihood estimation for dynamic and static longitudinal marginal structural working models. *Journal of causal inference* 2, 2 (2014), 147–185.

[45] Maya L Petersen, Kristin E Porter, Susan Gruber, Yue Wang, and Mark J Van Der Laan. 2012. Diagnosing and responding to violations in the positivity assumption. *Statistical methods in medical research* 21, 1 (2012), 31–54.

[46] Sophia M Rein, Jing Li, Miguel Hernan, and Andrew Beam. 2024. Deep Learning Methods for the Noniterative Conditional Expectation G-Formula for Causal Inference from Complex Observational Data. *arXiv preprint arXiv:2410.21531* (2024).

[47] James Robins. 1986. A new approach to causal inference in mortality studies with a sustained exposure period—application to control of the healthy worker survivor effect. *Mathematical modelling* 7, 9-12 (1986), 1393–1512.

[48] James Robins and Miguel Hernan. 2008. Estimation of the causal effects of time-varying exposures. *Chapman & Hall/CRC Handbooks of Modern Statistical Methods* (2008), 553–599.

[49] James M Robins. 2000. Marginal structural models versus structural nested models as tools for causal inference. In *Statistical models in epidemiology, the environment, and clinical trials*. Springer, 95–133.

[50] James M Robins, Andrea Rotnitzky, and Lue Ping Zhao. 1994. Estimation of regression coefficients when some regressors are not always observed. *Journal of the American statistical Association* 89, 427 (1994), 846–866.

[51] Paul R Rosenbaum and Donald B Rubin. 1983. The central role of the propensity score in observational studies for causal effects. *Biometrika* 70, 1 (1983), 41–55.

[52] Paul R Rosenbaum and Donald B Rubin. 1984. Reducing bias in observational studies using subclassification on the propensity score. *Journal of the American statistical Association* 79, 387 (1984), 516–524.

[53] Michael Rosenblum and Mark J Van Der Laan. 2010. Targeted maximum likelihood estimation of the parameter of a marginal structural model. *The international journal of biostatistics* 6, 2 (2010), 19.

[54] Daniel O Scharfstein, Andrea Rotnitzky, and James M Robins. 1999. Adjusting for nonignorable drop-out using semiparametric nonresponse models. *J. Amer. Statist. Assoc.* 94, 448 (1999), 1096–1120.

[55] Matthew Schlegel, Wesley Chung, Daniel Graves, Jian Qian, and Martha White. 2019. Importance resampling for off-policy prediction. *Advances in Neural Information Processing Systems* 32 (2019).

[56] Nabeel Seedat, Fergus Imrie, Alexis Bellot, Zhaozhi Qian, and Mihaela van der Schaar. 2022. Continuous-time modeling of counterfactual outcomes using neural controlled differential equations. *arXiv preprint arXiv:2206.08311* (2022).

[57] Toru Shirakawa, Yi Li, Yulun Wu, Sky Qiu, Yuxuan Li, Mingduo Zhao, Hiroyasu Iso, and Mark Van Der Laan. 2024. Longitudinal targeted minimum loss-based estimation with temporal-difference heterogeneous transformer. In *Proceedings of the 41st International Conference on Machine Learning*, 45097–45113.

[58] Jonathan M Snowden, Sherri Rose, and Kathleen M Mortimer. 2011. Implementation of G-computation on a simulated data set: demonstration of a causal inference technique. *American journal of epidemiology* 173, 7 (2011), 731–738.

[59] Ori M Stitelman, Victor De Gruttola, and Mark J van der Laan. 2012. A General Implementation of TMLE for Longitudinal Data Applied to Causal Inference in Survival Analysis. *The International Journal of Biostatistics* 8, 1 (2012), 1–39.

[60] Adam Stooke, Kimin Lee, Pieter Abbeel, and Michael Laskin. 2021. Decoupling representation learning from reinforcement learning. In *International conference on machine learning*. PMLR, 9870–9879.

[61] Elizabeth A Stuart. 2010. Matching methods for causal inference: A review and a look forward. *Statistical science: a review journal of the Institute of Mathematical Statistics* 25, 1 (2010), 1.

[62] Richard S Sutton, Andrew G Barto, et al. 1998. *Reinforcement learning: An introduction*. Vol. 1. MIT press Cambridge.

[63] Sarah L Taubman, James M Robins, Murray A Mittleman, and Miguel A Hernán. 2009. Intervening on risk factors for coronary heart disease: an application of the parametric g-formula. *International journal of epidemiology* 38, 6 (2009), 1599–1611.

[64] Philip Thomas and Emma Brunskill. 2016. Data-efficient off-policy policy evaluation for reinforcement learning. In *International conference on machine learning*. PMLR, 2139–2148.

[65] Philip Thomas and Emma Brunskill. 2016. Data-Efficient Off-Policy Policy Evaluation for Reinforcement Learning. In *Proceedings of The 33rd International Conference on Machine Learning (Proceedings of Machine Learning Research, Vol. 48)*, Maria Florina Balcan and Kilian Q. Weinberger (Eds.). PMLR, New York, New York, USA, 2139–2148. <https://proceedings.mlr.press/v48/thomasa16.html>

[66] Linh Tran, Constantin Yiannoutsos, Kara Wools-Kaloustian, Abraham Siika, Mark Van Der Laan, and Maya Petersen. 2019. Double robust efficient estimators of longitudinal treatment effects: comparative performance in simulations and a case study. *The international journal of biostatistics* 15, 2 (2019), 20170054.

[67] Mark J van der Laan and Susan Gruber. 2011. Targeted minimum loss based estimation of causal effects of multiple time point interventions. *International Journal of Biostatistics* 8, 1 (2011).

[68] Cameron Voloshin, Hoang M. Le, Nan Jiang, and Yisong Yue. 2021. Empirical Study of Off-Policy Policy Evaluation for Reinforcement Learning. *arXiv:1911.06854 [cs.LG]* <https://arxiv.org/abs/1911.06854>

[69] Shirley Wang, Matthew B. A. McDermott, Geeticka Chauhan, Marzyeh Ghassemi, Michael C. Hughes, and Tristan Naumann. 2020. MIMIC-Extract: a data extraction, preprocessing, and representation pipeline for MIMIC-III. In *Proceedings of the ACM Conference on Health, Inference, and Learning (ACM CHIL '20)*. ACM, 222–235. doi:10.1145/3368555.3384469

[70] Stanley Xu, Colleen Ross, Marsha A Raebel, Susan Shetterly, Christopher Blanchette, and David Smith. 2010. Use of stabilized inverse propensity scores as weights to directly estimate relative risk and its confidence intervals. *Value in Health* 13, 2 (2010), 273–277.

A Algorithm

A.1 LTMLE

We adopted the one-step LTMLE algorithm [67] and added an L1 regularizer for the targeting update [4].

Algorithm 3 LTMLE

1: **Input:** Dataset $\{O_i\}_{i=1}^n$; Initial estimates of Q_t and G_t for $t = 1, \dots, \tau$; L1 regularization coefficient: λ .
 2: **Output:** CAPO estimate $\hat{\psi}_n = \mathbb{P}_n Q_{1,\epsilon_1}(a_1, H_1)$
 3: Initialize $Q_{\tau+1} = Y$, $\epsilon_{\tau+1} = 0$
 4: Initialize submodel:

$$\text{logit}Q_{t,\epsilon_t} = \text{logit}Q_t + \epsilon_t$$
 and loss function

$$L_t(\epsilon_t) = \left(\prod_{s=1}^t \hat{w}_s(A_s, H_s) \right) \mathcal{L}_{bce}(Q_{t,\epsilon_t}(A_t, H_t), Q_{t+1,\epsilon_{t+1}}(a_{t+1}, H_{t+1})),$$
 where $\hat{w}_s = \frac{\mathbb{1}(A_s = a_s)}{A_s \cdot \hat{G}_s(H_s) + (1 - A_s)(1 - \hat{G}_s(H_s))}$.
 5:
 6: **for** $t = \tau$ to 1 **do**
 7: $\epsilon_t \leftarrow \arg \min_{\epsilon_t} \mathbb{P}_n L_t(\epsilon_t) + \lambda |\epsilon_t|$
 8: **end for**

B Proof

Lemma 4 (First- vs. second-order dependence in training targets). Assume bounded outcomes and positivity. Let \hat{Q}_t^{ICE} be the initial estimate from regular ICE G-computation, and let \hat{Q}_t^{SDR} be the initial estimate from SDR procedure. Throughout, we suppress function arguments when clear from context; e.g., Q_t^0 denotes $Q_t^0(A_t, H_t)$ and G_k^0 denotes $G_k^0(A_k | H_k)$ unless arguments are shown explicitly.

Then, for each $t = 1, \dots, \tau - 1$, the population regression errors admit the bounds

$$\begin{aligned} \|\hat{Q}_t^{\text{ICE}} - Q_t^0\|_2 &\leq \xi_t^{\text{ICE}} + \|\hat{Q}_{t+1}^{\text{ICE}}(a_{t+1}, H_{t+1}) - Q_{t+1}^0(a_{t+1}, H_{t+1})\|_2, \\ \|\hat{Q}_t^{\text{SDR}} - Q_t^0\|_2 &\leq \xi_t^{\text{SDR}} + \sum_{k=t+1}^{\tau} C_{t,k} \|\hat{G}_k^{\text{SDR}} - G_k^0\|_2 \|\hat{Q}_k^{\text{SDR}} - Q_k^{\dagger}\|_2, \end{aligned}$$

for constants $C_{t,k}$ depending only on positivity and τ , where ξ_t^{ICE} and ξ_t^{SDR} denotes the regression-to-target error at time t for corresponding estimator.

PROOF. Consider a deterministic treatment sequence $\mathbf{a} = (a_1, \dots, a_\tau)$. Recall the target regression at time t under \mathbf{a} :

$$Q_t^0(A_t, H_t) := \mathbb{E}[Q_{t+1}^0(a_{t+1}, H_{t+1}) \mid A_t, H_t].$$

Throughout, positivity means $G_k^0(H_k), \hat{G}_k^{\text{SDR}}(H_k) \in [\delta, 1 - \delta]$ a.s. for all $k \in [\tau]$, so all density ratios below are uniformly bounded.

Step 1: a generic decomposition. For any training target T_{t+1} (measurable w.r.t. (H_{t+1}, A_{t+1})), define its conditional mean

$$m_t^T(A_t, H_t) := \mathbb{E}[T_{t+1} \mid A_t, H_t].$$

Then by the triangle inequality,

$$\|\hat{Q}_t - Q_t^0\|_2 \leq \underbrace{\|\hat{Q}_t - m_t^T\|_2}_{:= \xi_t} + \|m_t^T - Q_t^0\|_2. \quad (8)$$

We apply (8) to the ICE target and the SDR target separately.

Step 2: ICE target yields a first-order bias term. For ICE, the training target is

$$T_{t+1}^{\text{ICE}} := \hat{Q}_{t+1}^{\text{ICE}}(a_{t+1}, H_{t+1}).$$

Hence

$$m_t^{\text{ICE}} - Q_t^0 = \mathbb{E}[\hat{Q}_{t+1}^{\text{ICE}}(a_{t+1}, H_{t+1}) - Q_{t+1}^0(a_{t+1}, H_{t+1}) \mid A_t, H_t].$$

By Jensen (equivalently, $\|\mathbb{E}[U \mid A_t, H_t]\|_2 \leq \|U\|_2$),

$$\|m_t^{\text{ICE}} - Q_t^0\|_2 \leq \|\hat{Q}_{t+1}^{\text{ICE}}(a_{t+1}, H_{t+1}) - Q_{t+1}^0(a_{t+1}, H_{t+1})\|_2.$$

Combining this with (8) proves the ICE bound.

Step 3: SDR target yields a second-order bias term. For SDR, the training target is

$$T_{t+1}^{\text{SDR}} := Q_t^\dagger(a_{t+1}, H_{t+1}),$$

where Q^\dagger is constructed via (7) using nuisance estimates $(\hat{Q}^{\text{SDR}}, \hat{G}^{\text{SDR}})$.

Let

$$m_t^{\text{SDR}}(A_t, H_t) := \mathbb{E}[Q_{t+1}^\dagger(a_{t+1}, H_{t+1}) \mid A_t, H_t].$$

We will bound $\|m_t^{\text{SDR}} - Q_t^0\|_2$.

Define the (true and estimated) density ratios for the fixed sequence \mathbf{a} :

$$\begin{aligned} w_k^0(A_k, H_k) &:= \frac{\mathbb{1}(A_k = a_k)}{A_k G_k^0(H_k) + (1 - A_k)(1 - G_k^0(H_k))}, \\ \hat{w}_k(A_k, H_k) &:= \frac{\mathbb{1}(A_k = a_k)}{A_k \hat{G}_k^{\text{SDR}}(H_k) + (1 - A_k)(1 - \hat{G}_k^{\text{SDR}}(H_k))}. \end{aligned}$$

Under positivity, $\|\hat{w}_k\|_\infty \vee \|w_k^0\|_\infty \leq \delta^{-1}$ and

$$\|\hat{w}_k - w_k^0\|_2 \lesssim \|\hat{G}_k^{\text{SDR}} - G_k^0\|_2. \quad (9)$$

Now consider the difference between the SDR pseudo-outcome and its population counterpart. Lemma 3 in Díaz et al. [12] implies that, for each fixed t ,

$$m_t^{\text{SDR}} - Q_t^0 = \sum_{k=t+1}^{\tau} \mathbb{E}[W_{t,k}(\hat{w}_k - w_k^0)(\hat{Q}_k^{\text{SDR}} - Q_k^\dagger) \mid A_t, H_t], \quad (10)$$

where $W_{t,k}$ is a product of (true and/or estimated) weight factors over times $t+1, \dots, k-1$. By positivity, $\|W_{t,k}\|_\infty \leq C'_{t,k}$ for constants $C'_{t,k}$ depending only on (δ, τ) .

Apply Jensen and Cauchy-Schwarz to (10):

$$\begin{aligned} \|m_t^{\text{SDR}} - Q_t^0\|_2 &\leq \sum_{k=t+1}^{\tau} \left\| \mathbb{E}[W_{t,k}(\hat{w}_k - w_k^0)(\hat{Q}_k^{\text{SDR}} - Q_k^\dagger) \mid A_t, H_t] \right\|_2 \\ &\leq \sum_{k=t+1}^{\tau} \|W_{t,k}\|_\infty \|(\hat{w}_k - w_k^0)(\hat{Q}_k^{\text{SDR}} - Q_k^\dagger)\|_2 \\ &\leq \sum_{k=t+1}^{\tau} C'_{t,k} \|\hat{w}_k - w_k^0\|_2 \|\hat{Q}_k^{\text{SDR}} - Q_k^\dagger\|_2. \end{aligned}$$

Invoking (9) yields

$$\|m_t^{\text{SDR}} - Q_t^0\|_2 \leq \sum_{k=t+1}^{\tau} C_{t,k} \|\hat{G}_k^{\text{SDR}} - G_k^0\|_2 \|\hat{Q}_k^{\text{SDR}} - Q_k^\dagger\|_2,$$

for constants $C_{t,k}$ depending only on (δ, τ) . Finally, combine this bound with the generic decomposition (8) (with $T = T^{\text{SDR}}$), where $\xi_t = \|\hat{Q}_t^{\text{SDR}} - m_t^{\text{SDR}}\|_2$, to obtain the SDR inequality in the theorem. \square

C Experiment Setting

C.1 Baseline Implementation

We implement G-computation and LTMLE with Super Learner using the `ltmle` R package, setting `gcomp=TRUE` for the former. Super Learner constructs an optimally weighted ensemble of base learners via k -fold cross-validation; throughout, we set $k = 3$ and include a generalized linear model, random forest, XGBoost, and a generalized additive model (GAM) with regression splines as candidate learners. Since these two models do not support applying the fitted model to a hold-out validation set, we feed all 1500 samples to the models for both training and inference.

DeepACE is implemented using the authors' original codebase [17]. Across 20 runs, a small number of runs (1–3, depending on the DGP and counterfactual policy) produced substantially divergent estimates; these runs were excluded from the reported results, which favors DeepACE's performance.

For DeepLTMLE, we follow the original paper to derive our own implementation. Additionally, while the author proposes using no activation function after the linear layer of their Q -head for continuous outcomes, we observed substantial divergence in the experiment under this practice. Therefore, we used a sigmoid activation to stabilize their optimization, similar to our implementation. This modification favors DeepLTMLE's performance. For D^3 -Net, we begin with DeepLTMLE's heterogeneous transformer architecture, where inputs are first passed through a type-embedding layer distinguishing covariates L , treatment A , and outcome Y , and combined with positional encodings. The resulting embedding is processed by a Transformer block, whose output feeds into a Q -head for outcome regression, and M G -heads and S -heads for next- M -step treatment and covariate predictions. All 'heads' are a linear layer followed by an activation function. Q uses sigmoid activation as the outcome is bounded between 0 and 1; G uses sigmoid as the treatment is binary; S uses none, as the covariates in our experiments are all continuous. The Polyak averaging coefficient is set to $\beta = 0.02$. All deep learning models, including DeepACE, DeepLTMLE, and our proposed method, are trained for 100 epochs.

Table S1: Absolute bias (mean \pm std) and RMSE of CAPO estimates at horizon $\tau = 10$.

Model	Limited Time-varying Confounding								Expanded Time-varying Confounding							
	Bias				RMSE				Bias				RMSE			
	CF 1	CF 2	CF 3	CF 4	CF 1	CF 2	CF 3	CF 4	CF 1	CF 2	CF 3	CF 4	CF 1	CF 2	CF 3	CF 4
G-comp (sl.)	2.72 \pm 1.59	3.70 \pm 1.39	3.13 \pm 0.98	4.14 \pm 1.47	3.13	3.94	3.27	4.38	1.74 \pm 0.94	3.28 \pm 1.26	1.86 \pm 0.82	3.27 \pm 1.06	1.96	3.50	2.02	3.43
LTM. (sl.)	2.80 \pm 1.30	3.29 \pm 1.78	0.24\pm 0.22	0.55 \pm 0.32	3.08	3.72	0.32	0.64	1.92 \pm 1.10	3.22 \pm 1.56	0.17\pm 0.13	0.36 \pm 0.21	2.20	3.56	0.21	0.41
DACE	1.14 \pm 0.12	0.80\pm 0.12	0.91 \pm 0.57	0.63 \pm 0.46	1.14	0.81	1.06	0.77	1.24 \pm 0.11	0.95 \pm 0.11	0.95 \pm 0.35	0.83 \pm 0.36*	1.24	0.95	1.01	0.90
D.LTMLE	1.13\pm1.25	1.71 \pm 0.72	0.73 \pm 0.24	0.44 \pm 0.34	1.66	1.84	0.77	0.55	1.29 \pm 1.08	1.40 \pm 0.60	0.69 \pm 0.33	0.32 \pm 0.22	1.67	1.51	0.76	0.39
D^3 -Net	0.73\pm0.47	0.83 \pm 0.41	0.61 \pm 0.27	0.23\pm 0.15	0.86	0.92	0.67	0.27	0.53\pm0.54	0.92\pm0.59	0.49\pm0.27	0.21 \pm 0.13	0.74	1.08	0.56	0.25

C.2 Semi-Synthetic Data DGP

DGP with Limited Time-varying Confounding We adopt the semi-synthetic DGP from DeepACE. Using the preprocessing pipeline of Wang et al. [69], we extract 10 time-varying covariates $X_t \in \mathbb{R}^{10}$ over $\tau = 15$ time steps. These covariates are treated as observed patient states and are directly taken from real-world measurements.

Given the observed history, binary treatments $A_t \in \{0, 1\}$ are simulated according to a stochastic, dynamic treatment policy. The treatment assignment probability at time t depends on past covariates, past intermediate outcomes, and a treatment intensity variable $\ell_t = \ell_{t-1} + 2(A_t - 1)\bar{X}_t \tanh(Y_t)$, with initialization $\ell_0 = T/2 - 3$. Treatment is assigned as

$$\pi_t = \mathbb{1} \left\{ \sigma \left(\sum_{i=1}^h \frac{(-1)^i}{1-i} \left(\bar{X}_{t-i} + \frac{\tanh(Y_{t-i})}{2} \right) \right. \right. \\ \left. \left. - \tanh \left(\ell_{t-1} - \frac{T}{2} \right) + \epsilon_t^A \right) > 0.5 \right\},$$

and outcomes are generated according to

$$Y_{t+1} = 5 \sum_{i=1}^h \frac{(-1)^i}{1-i} \tanh(\sin(\bar{X}_{1:5,t-i} A_{t-i}) + \cos(\bar{X}_{5:10,t-i} A_{t-i})) + \epsilon_t^Y,$$

where $\bar{X}_{1:5,t-i}$ represent the mean of the first five covariates at step $t-i$, similarly for $\bar{X}_{5:10,t-i}$. The time lag $h = 8$. Noise terms satisfy $\epsilon_t^A, \epsilon_t^Y \sim \mathcal{N}(0, 0.5^2)$.

Our target estimand is the terminal outcome Y_{15} . Intermediate outcomes Y_t for $t < 15$ are absorbed into L_{t+1} (Section 5.1), yielding $L_t = (X_t, Y_{t-1})^\top \in \mathbb{R}^{11}$.

DGP with Expanded Time-varying Confounding In the simple DGP above, patient covariates are unaffected by treatment. To introduce a stronger and more realistic treatment-confounder feedback loop, we further synthesize treatment-dependent time-varying covariates.

Specifically, we generate latent covariates $Z_t \in \mathbb{R}^5$ with initialization $Z_1 \sim \mathcal{N}(0, I)$ and dynamics

$$Z_{t+1} = \omega_1 \cdot Z_t + \omega_2 \cdot A_t \sigma(Z_t^2) + \omega_3 \cdot 0.25 \tanh(\bar{X}_t) + \epsilon_t^Z,$$

where $\epsilon_t^Z \sim \mathcal{N}(0, 0.3^2)$ and the coefficients $\omega = (\omega_1, \omega_2, \omega_3)$ are randomly drawn and fixed to $(0.37, 0.42, 0.29)$. These synthesized covariates both affect and are affected by treatment.

We concatenate Z_t with the observed covariates to form the augmented state

$$X_t^\dagger = (X_t, Z_t)^\top \in \mathbb{R}^{15}.$$

Treatment assignment and outcome generation follow the same structural equations as in the Simple Semi-synthetic DGP, with X_t replaced by X_t^\dagger . Noise distributions remain unchanged.

Table S2: Hyperparameter tuning grid used for all datasets and counterfactual settings.

Hyperparameter	DeepACE	DeepLTMLE	D^3 -Net
Batch size	{128, 256}	{128, 256}	{128, 256}
Learning rate	{5e-4, 1e-3, 5e-3}	{5e-4, 1e-3, 5e-3}	{5e-4, 1e-3, 5e-3}
Hidden size	{8, 16, 32}	{8, 16, 32}	{8, 16, 32}
Dropout rate	{0.0, 0.1}	{0.0, 0.1}	{0.0, 0.1}
Number of layers	—	{1, 2, 3}	{1, 2, 3}
Number of heads	—	{2, 4}	{2, 4}
α	—	{0.5, 1.0}	{0.5, 1.0}

C.3 Hyperparameter Tuning

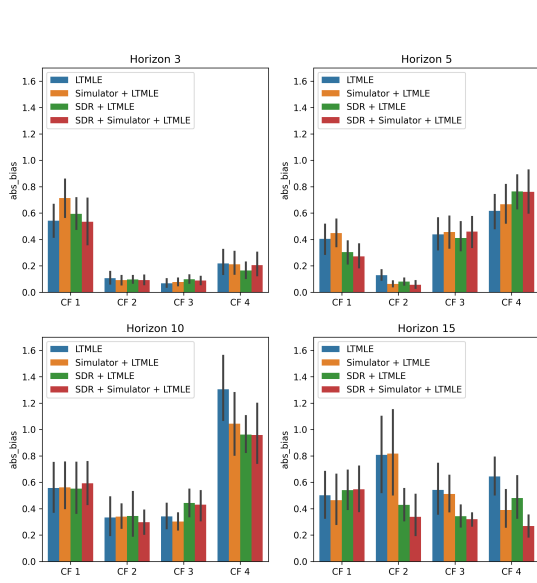
Using this horizon, we allocate 800 trajectories for training and 200 for validation to tune hyperparameters of all baselines (Appendix C.3). Using the optimal hyperparameter, models are retrained on the combined set of 1000 trajectories and evaluated on a held-out test set of 500 trajectories. The same sample-splitting protocol is applied across all methods to ensure comparability. We use the same 1000/500 train-eval split for $\tau = 10$ and $\tau = 20$, but skip the hyperparameter tuning and reuse those selected at $\tau = 15$.

We use the random search strategy to tune the hyperparameters for all models. Since we only have factual data, we select hyperparameters by minimizing the factual loss: $L_{mse}(Q(A_t, H_t), Y) + \sum_{t=1}^{\tau} L_{bce}(G(H_t), A_t)$. Table S2 presents the hyperparameter grid.

C.4 Counterfactuals

We consider four counterfactual treatment sequences for each horizon: never treat, always treat, treat in the first half of the horizon, and treat in the second half of the horizon. Specifically,

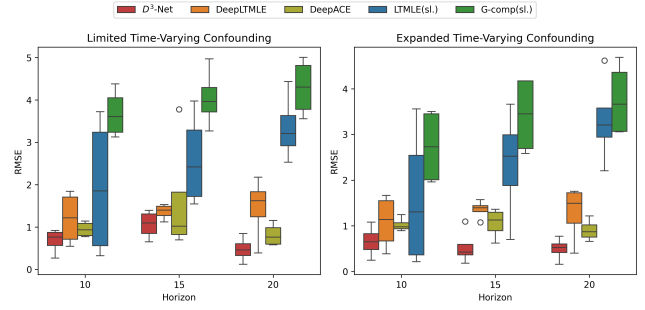
- $\tau = 20$: **CF 1** = $a_t = 0$ for t in 1 to τ ; **CF 2** = $a_t = 1$ for t in 1 to τ ; **CF 3** = $a_t = 1$ for t in 1 to 10 and $a_t = 0$ for t in 11 to τ ; **CF 4** = $a_t = 0$ for t in 1 to 10 and $a_t = 1$ for t in 11 to τ
- $\tau = 15$: **CF 1** = $a_t = 0$ for t in 1 to τ ; **CF 2** = $a_t = 1$ for t in 1 to τ ; **CF 3** = $a_t = 1$ for t in 1 to 10 and $a_t = 0$ for t in 11 to τ ; **CF 4** = $a_t = 0$ for t in 1 to 5 and $a_t = 1$ for t in 11 to τ
- $\tau = 10$: **CF 1** = $a_t = 0$ for t in 1 to τ ; **CF 2** = $a_t = 1$ for t in 1 to τ ; **CF 3** = $a_t = 1$ for t in 1 to 5 and $a_t = 0$ for t in 6 to τ ; **CF 4** = $a_t = 0$ for t in 1 to 5 and $a_t = 1$ for t in 6 to τ
- $\tau = 5$: **CF 1** = $a_t = 0$ for t in 1 to τ ; **CF 2** = $a_t = 1$ for t in 1 to τ ; **CF 3** = $a_t = 1$ for t in 1 to 3 and $a_t = 0$ for t in 4 to τ ; **CF 4** = $a_t = 0$ for t in 1 to 2 and $a_t = 1$ for t in 3 to τ
- $\tau = 3$: **CF 1** = $a_t = 0$ for t in 1 to τ ; **CF 2** = $a_t = 1$ for t in 1 to τ ; **CF 3** = $a_t = 1$ for t in 1 to 2 and $a_t = 0$ for $t = \tau$; **CF 4** = $a_t = 0$ for $t = 1$ and $a_t = 1$ for t in 2 to τ

Figure S2: Ablation study on training components of $D^3\text{-Net}$.

D Additional Results

D.1 Main Experiments

We summarize the RMSE distribution across counterfactual sequences under different horizons and confoundings in Figure S1.

Figure S1: RMSE of CAPO estimates across counterfactual sequences for horizons $\tau \in 10, 15, 20$ under limited (left) and expanded (right) time-varying confounding.

D.2 Ablation Studies

With LTMLE in place, we ablate the two training components on the dataset with expanded time-varying confounding across different horizons and counterfactual sequences. Figure S2 shows detailed results across counterfactual sequences and horizon.

E Extension to dynamic treatment regime

Following prior work such as DeepLTMLE, our framework naturally extends to estimating the CAPO of dynamic treatment regimes (policies) without any architectural modification, since both methods are built on the ICE G-computation principle. We refer readers to Shirakawa et al. [57] for a detailed derivation of policy evaluation under ICE G-computation.

We briefly summarize the implementation-level change required for policy evaluation. Let a policy be denoted by $\boldsymbol{\pi} = (\pi_1, \dots, \pi_\tau)$, where each decision rule π_t maps the observed history h_t to a treatment assignment. In the pseudo-outcome generation step of ICE G-computation (or its SDR variant), instead of feeding a fixed deterministic counterfactual action a_t at time t , we evaluate the nuisance models at the policy-prescribed action $\pi_t(h_t)$. Concretely, all occurrences of a_t in the recursive target construction are replaced by $\pi_t(h_t)$, so that the backward recursion propagates counterfactual outcomes under the policy $\boldsymbol{\pi}$ rather than under a fixed treatment sequence.

This modification yields an estimator of the CAPO under the dynamic regime $\boldsymbol{\pi}$, while leaving the network architecture and training procedure unchanged.